ADVANCED FUNCTIONAL MATERIALS
www.afm-journal.de

Multiple Layer-by-Layer Lipid-Polymer Hybrid Nanoparticles for Improved FOLFIRINOX Chemotherapy in Pancreatic Tumor Models

Feng Li, Xiao Zhao, Hai Wang, Ruifang Zhao, Tianjiao Ji, He Ren, Gregory J. Anderson, Guangjun Nie, and Jihui Hao**

The FOLFIRINOX regimen, a combination of three chemotherapy agents (5-fluorouracil, irinotecan, oxaliplatin) and folinic acid (a vitamin B derivatives reducing the side effect of 5-fluorouracil), has proved to be effective in the treatment of pancreatic cancer, and is more efficacious than the long-term reference standard, gemcitabine. However, the FOLFIRINOX is associated with high-grade toxicity, which markedly limits its clinical application. Encapsulation of drugs in nanocarriers that selectively target cancer cells promises to be an effective method for co-delivery of drug combinations and to mitigate the side effects of conventional chemotherapy. Here we reported the development of multiple layer-by-layer lipid-polymer hybrid nanoparticles with targeting capability that show excellent biocompatibility and synergistically combine the favorable properties of liposomes and polymer nanoparticles. Relative to nanoparticles consisting of polymer alone, these novel nanocarriers have a long half-life in vivo and a higher stability in serum. The nanocarriers were loaded with the three active antitumor constituents of FOLFIRINOX regimen. Little drugs were released from the nanoparticles in phosphate buffered saline (PBS) solution, but the cargoes were quickly released after the nanoparticles were taken up by tumor cells. These innovative drug-loaded nanoparticles achieved higher antitumor efficacy and showed minimal side effects compared with the FOLFIRINOX regimen alone. Our study suggested that the multiple layer-by-layer hybrid nanoparticles have great potential for improving the chemotherapeutic efficacy for the patients with pancreatic cancer. This platform also provides new opportunities for tailored design of nanoparticles that may offer therapeutics benefits for a range of other tumors.

1. Introduction

Pancreatic ductal adenocarcinoma is one of the most lethal human malignancies with a 5-year survival rate of less than 5%.[1] In recent decades, treatment with gemcitabine has become the standard for advanced pancreatic cancer.[2] However, the median overall survival with gemcitabine as the sole therapy is only about 5–7 months.[3] Almost all phase III studies of combinations between gemcitabine and other chemotherapeutic drugs have given disappointing results, with either no improvement in efficacy or unacceptable toxicity.[4–6] The most successful drug combination tried to date is FOLFIRINOX, a combination of 5-fluorouracil (5-Fu), irinotecan (Camptosar, CPT), oxaliplatin (Oxa), and folinic acid (a vitamin B derivatives reducing the side effect of 5-Fu). Relative to gemcitabine, FOLFIRINOX significantly prolongs survival in patients with metastatic pancreatic adenocarcinoma (median survival of 11.1 vs 6.8 months, $P < 0.01$).[7] However, FOLFIRINOX significantly reduces the quality of life in those patients as a result of a range of undesirable and severe side effects, including neutropenia, febrile neutropenia, thrombocytopenia, diarrhea, and sensory neuropathy.[7,8] These have seriously hindered its development as the new standard first-line option for most patients of pancreatic cancer.[9,10] Therefore, a strategy that could simultaneously maintain (or improve) its therapeutic efficacy, yet decrease the toxicity of FOLFIRINOX would represent a major development in the chemotherapy for advanced pancreatic cancer.

Targeted delivery of drugs using nanotechnology has shown great promise for improving cancer treatment. To date, approximately 150 nanotechnology-based cancer therapeutic drugs are in various stages of development, along with some drugs widely used in the clinic.[11–13] For pancreatic cancer treatment, Von Hoff et al. (in the MPACT study) showed that patients treated with gemcitabine together with Abraxane (a nanotechnology-based drug, also known as nab-paclitaxel) had significantly longer overall survival than the patients treated with gemcitabine alone (median survival of 8.5 vs 6.7 months,

F. Li, X. Zhao, Dr. H. Ren, Prof. J. Hao
Department of Pancreatic Carcinoma
Tianjin Medical University Cancer Institute and Hospital
National Clinical Research Center of Cancer
Key Laboratory of Cancer Prevention and Therapy
Tianjin 300060, China
E-mail: haojihui@tjmuch.com

F. Li, X. Zhao, Dr. H. Wang, R. Zhao, T. Ji, Prof. G. Nie
CAS Key Laboratory for Biomedical Effects of Nanomaterials and Nanosafety
National Center for Nanoscience and Technology (NCNST)
11 Beiyitiao, Zhongguancun, Beijing 100190, China
E-mail: niegj@nanoctr.cn

Prof. G. J. Anderson
Iron Metabolism Laboratory
QIMR Berghofer Medical Research Institute
Brisbane, Queensland 4029, Australia

DOI: 10.1002/adfm.201401583

$P < 0.001$).[14] Nanoparticles encapsulation is the most widely used nanotechnology in drug delivery. Nanoparticles containing chemotherapeutic drugs potentially can overcome some problems associated with conventional "free" drugs, including poor solubility, low bioavailability, limited stability, fast renal clearance, development of drug resistance and/or, in particular, lack of selectivity, which can result in non-specific toxicity to normal cells and prevent the dose escalation.[15] The ideal nanoparticles allow effective encapsulation of the drug cargoes and enable tailored controlled release of drugs in the diseased area. The rational design of drug nanocarriers by surface modification and/or by controlling their size or shape allows them to overcome various extra- and intra-cellular barriers before they reach the tumor sites where the therapeutic agents are released.[13]

Liposomes and polymers are the dominant materials used in the fabrication of drug-containing nanoparticles.[16,17] These components are, in general, biodegradable and biocompatible, and readily available. The nanoparticles allow drugs to be delivered with high efficiency, and in a targeted fashion via enhanced vascular access of tumor tissues and/or active targeting strategy with tumor targeting motifs on their surface, which ensures that side effects are minimized compared with free drug administration.[16,18] Liposomes are highly biocompatible and are able to interact with a wide variety of molecules due to their amphiphilic nature. In addition, the liposome surface can be functionalized readily with hydrophilic polymers, such as poly(ethylene glycol) (PEG), to prolong the plasma half-life and to link targeting molecules to the particle surface to enable better accumulation in the targeted tumor sites.[17,19] However, liposomes have some less desirable characteristics. The efficiency of drug encapsulation is often low and liposomes are susceptible to disruption by osmotic stress and shear forces.[20] Polymer nanoparticles show a number of favorable characteristics for drug delivery which complement those of liposomes. They are able to encapsulate drugs with high capacity, and show strong structural stability.[16] Unfortunately, polymer nanoparticles also have their negative features. For example, these particles are often heterogeneous and are easily hydrolyzed; their surface can only be functionalized at low density and the cargoes are prone to drug leakage before reaching diseased area.[21–23]

Hybrid lipid-polymer nanocomposites, with a single layer or bilayer lipid shell around a polymer core, may combine the advantages of polymer particles with the best attributes of liposomes for drug delivery applications. Efficient drug encapsulation can be achieved both in the polymeric core and in the lipid shell, and drug release can be controlled by both polymer degradation and by the presence of the lipid coat which acts as a diffusion barrier.[24] The lipid shell provides a good platform for further surface functionalization, and such particles would be predicted to have improved stability and potential enriched biological functionality. Although the potential applications of lipid-polymer hybrid nanoparticles technology to overcome some of the significant issues associated with chemotherapeutics is huge, the development of methods for the formulation of lipid-polymer hybrid nanoparticles remains in its infancy.[16,25] In particular, there are no reports of hybrid lipid-polymer nanocarriers being used for three or more drugs with different physicochemical properties. Herein, our study has showed a great success of such a novel strategy for simultaneously loading multiple chemotherapeutics and mitigating the toxicity associated with FOLIRINOX treatment, with an even enhanced antitumor efficacy in pancreatic tumor models.

In the present study, we have extended our previous studies[26,27] to develop targeted multiple layer-by-layer lipid-polymer hybrid nanoparticles composed of a polymeric core and a PEGylated lipid shell. We have used these for the simultaneous delivery of the three effective constituents of FOLFIRINOX, the two hydrophilic drugs 5-Fu and Oxa, and the hydrophobic drug CPT. The solid polymeric core acts as a scaffold to encapsulate both hydrophilic and hydrophobic drugs. The lipid shell enveloping the core prevents drug leakage and contains the drugs until the nanoparticles enter the target cells.

2. Results and Discussion

2.1. Preparation and Characterization of Lipid-Polymer Hybrid Nanoparticles

The lipid-polymer hybrid nanoparticles were fabricated reproducibly by combining an improved double emulsion method for polymer nanoparticles fabrication and the ultrasound assisted self-assembly of a lipid film.[26,28] The internal polymer components were constructed based on methoxy polyethylene glycol (mPEG) and polylactide (PLA), two well-characterized and biodegradable materials widely used for in vitro and in vivo drug delivery and approved for clinical use by the US Food and Drug Administration.[29] The diblock copolymer mPEG-PLA was synthesized as described previously.[30] Nuclear magnetic resonance (NMR) and Fourier transform infrared spectroscopy (FTIR) measurement confirmed the successful synthesis of mPEG-PLGA copolymer (Figure S1, Supporting Information). We then prepared the polymeric nanocore through an improved double emulsion strategy (**Scheme 1**).[26,28] This method uses a two-step process to prepare a water-in-oil emulsion, followed by generating a water-in-oil-in-water emulsion using surfactants to form polymeric nanoparticles (PNPs). Encapsulation of a drug through a traditional double emulsion can be achieved when the drug is soluble in the inner aqueous phase. To load a hydrophobic drug, it can be introduced into the hydrophobic layer with an improved double emulation method. Therefore, both hydrophobic and hydrophilic drugs can be loaded in the same nanocarriers simultaneously.

A mixture of phospholipids and cholesterol [lecithin, 1,2-distearoyl-sn-glycero-3-phosphoethanolamine-*N*-[methoxy(polyethylene glycol)-2000] (DSPE-PEG-2000), 1,2-distearoyl-sn-glycero-3-phosphoethanolamine-*N*-[maleimide(polyethylene glycol)-3400] (DSPE-PEG-3400-Mal) and cholesterol in a 60:10:2:15 mass ratio] formed lipid film, was then used to coat the polymeric core by self-assembly of the lipid film under ultrasound to form lipid-polymer hybrid nanoparticles (LPNPs). The tumor targeting polypeptide Arg-Gly-Asp (RGD) motif, which specifically recognizes the *avb*3 integrin overexpressed on various tumor cells and tumor-derived endothelial cells, was linked covalently to the PEGylated lipid through reaction between sulfhydryl and maleimide groups.[31] The resulting targeted lipid-polymer hybrid nanoparticles

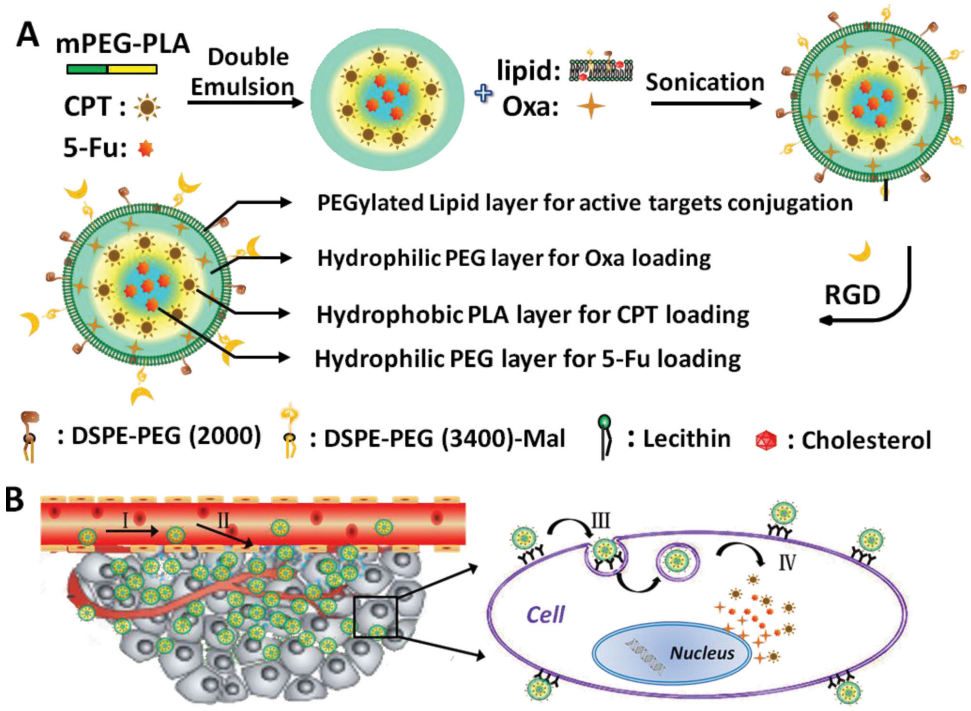

Scheme 1. Scheme of drug loading of hybrid nanoparticles A) and the proposed blood circulation and intracellular uptake and drugs release B). A) Schematic representation of the preparation of T-LPNPs with a multiple layer-by-layer structure. B) Schematic illustration of the process of T-LPNPs circulation in the blood with a long circulation life (I) and accumulation at the site of a tumor through the enhanced access of tumor blood vessel and active targeting (II). Subsequently, internalization of the T-PLNPs occurs (III), and the drugs rapidly released inside the cell (IV). 5-fluorouracil, 5-Fu; irinotecan, CPT; oxaliptatin, Oxa.

(T-LPNPs) consisted of multiple layers of mPEG-PLA core and a bilayer of PEGylated lipid shell, decorated with active tumor targeting RGD peptides (Scheme 1).

In the improved double emulsion method, 5-Fu was packaged within the hydrophilic core of the PNPs, while CPT was inserted into the hydrophobic layer (Scheme 1). Oxa will be wrapped at the interface of the surface lipid and polymeric core by mixing the pre-prepared polymer nanoemulsion with an aqueous solution of Oxa, followed by lipid bilayer coating on the PNPs by sonication (Scheme 1). We hypothesized that the encapsulation of the three antitumor drugs together would greatly increase efficacy, as the agents would most likely reach the tumor sites simultaneously. Oxa functions by forming both inter- and intra-strand cross links in DNA, CPT prevents DNA from unwinding by inhibition of topoisomerase, and 5-Fu acts principally as a thymidylate synthase inhibitor and blocks the synthesis of the thymidine required for DNA replication.[32,33]

We then examined whether a lipid bilayer assembled effectively on the surface of the polymeric core. Various weight ratios of lipid/polymer were explored (**Figure 1**a and Figure S2, Supporting Information). When the lipid/polymer ratio was as low as 0.05/1, there was a paucity of lipids on the surface of the PNPs, resulting in a zeta potential of –14.5 mV, close to that of bare PNPs (Figure S2A, Supporting Information). When the weight ratio reached up to 0.30/1, the lipid bilayer lipid effectively coated the surface of the polymer nanoparticles as the zeta potential changed gradually to –25.0 from –14.5 mV (Figure 1A). When the lipid/polymer weight ratio increased, the zeta potential peak at –14.5 mV decreased, and then disappeared (Figure 1A). There was a concomitant increase in the peak at approximately –25.0 mV. The size of the particles did not change significantly with the lipid coating (Figure 1A).

The morphology and structure of lipid-polymer hybrid nanoparticles was characterized by transmission electron microscopy (TEM) (Figure 1B). The hybrid nanoparticles were dispersed, with a well-defined spherical core-shell structure, and an average hydrodynamic diameter (as determined by DLS) of approximately 160 nm (Figure 1A). A multilayer structure can be observed clearly (Figure 1B). When we increased the molecular weight of PLA (from 15 000 to 30 000), the middle hydrophobic layer (marked as a in Figure S3B, Supporting Information) was thicker significantly (from about 15 nm to 35 nm). We hypothesize that this layer in Figure 1B may be the hydrophilic layer formed by PLA. When we increased the molecular weight of PLA (from 15 000 to 30 000), the middle hydrophobic layer (marked as a in Figure S3B, Supporting Information) was thicker significantly (from about 15 nm to 35 nm). We hypothesize that this layer in Figure 1B may be the hydrophilic layer formed by PLA.

2.2. The Stability of LPNPs in Vitro and in Vivo

The stability of LPNPs in serum was investigated by dissolving the nanoparticles in 10% fetal bovine serum (FBS) at room

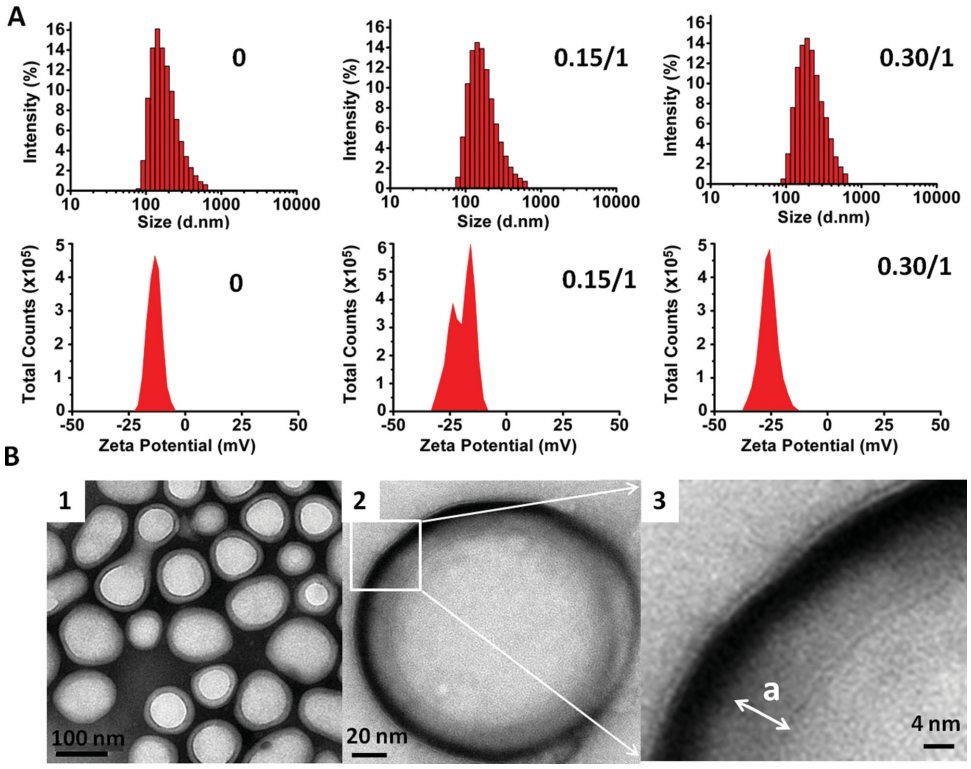

Figure 1. The size, zeta potential, and TEM images of LPNPs. A) Changes in the size and zeta potential of PNPs after modification with different amount of lipids (lipids/mPEG-PLA at 0/1, 0.15/1, 0.30/1, respectively). B) TEM image of the structure of the hybrid LPNPs. Uranyl acetate was used to stain lipids to enhance their contrast. 1 and 2 are at different magnifications. The inset marked in 2 is shown at higher magnification in 3 (a, the hydrophobic layer).

temperature and examining the size of the particles by DLS over time (**Figure 2**A). There was no significant change in the size distribution of LPNPs, even after 72 h incubation, but bare PNPs treated in the same way were of a much larger size and broader particle size distribution. This implies that the external lipid shell provides the better stability of the LPNPs in serum. As shown previously in Figure 1A, by coating of lipid bilayer, the zeta potential of LENPs changed from –14.5 to –25 mV. The enhanced surface negative charge increased repulsive force between the individual LPNP, which made them hard to aggregate. In addition, the lipid bilayer shell reduces possible penetration of serum components into the polymeric core. All factors together lead to decrease the rate of hydrolysis of mPEG-PLA and contribute to the stability of LPNPs in the serum.

To examine LPNPs stability in vivo, we loaded the fluorescent probe rhodamine B (RhoB) into PNPs (PNP-RhoB) and LPNPs (LPNP-RhoB). BALB/c Mice were separated into three groups and injected intravenously with free RhoB, PNP-RhoB, or LPNP-RhoB. At various time points after administration of the fluorescent preparations, blood was withdrawn from tail veins for fluorescent imaging (Figure 2B). Free RhoB disappeared rapidly from the circulation with fluorescence intensity reduced by half within 2 h, as did PNP-RhoB, but 63% of the LPNP-RhoB remained after 5 h. These data suggest that LPNPs had a prolonged half-life in vivo, a desirable characteristic for enhanced nanoparticles designed for cancer therapeutic drugs delivery.

2.3. Drug Loading and Release Studies in Vitro

High drug loading and controlled release of drugs are advantages of drug-loaded nanoparticles as they improve bioavailability and reduce the toxicity of the drugs to normal tissues. We confirmed the successful encapsulation of the drugs in LPNPs by high performance liquid chromatography (HPLC) spectra (Figure S4A and S4B, Supporting Information), as the drugs-loaded LPNPs had the characteristic absorption bands of 5-Fu, CPT, and Oxa. Then the drug encapsulation yields were examined (Figure S4C, Supporting Information), and the results showed the hybrid LPNPs were effective for co-delivery of hydrophilic and hydrophobic drugs, especially the CPT encapsulation efficiency could be as high as 96%, and the highest encapsulation efficiencies of 5-Fu and Oxa were 22.6% and 26.3%, respectively. The size distribution of LPNP-Drugs was similar with LPNPs (Figure S4D, Supporting Information) according to the DLS results.

The release profiles of LPNP-5-Fu-CPT-Oxa (LPNPs encapsulating 5-Fu, CPT, and Oxa) and PNP-5-Fu-CPT (PNPs encapsulating 5-Fu and CPT) in vitro were obtained at pH 7.4 and pH 4.4 at room temperature (Figure 2C). The lower pH was chosen as the nanoparticles are mainly taken up by cells and eventually transferred into lysosomes (pH 4–5), followed by degradation. The drug release profiles of PNP-5-Fu-CPT were pH-dependent,[23] with more rapid release being observed at pH 4.4. Nevertheless, even at pH 7.4, most of the drugs were

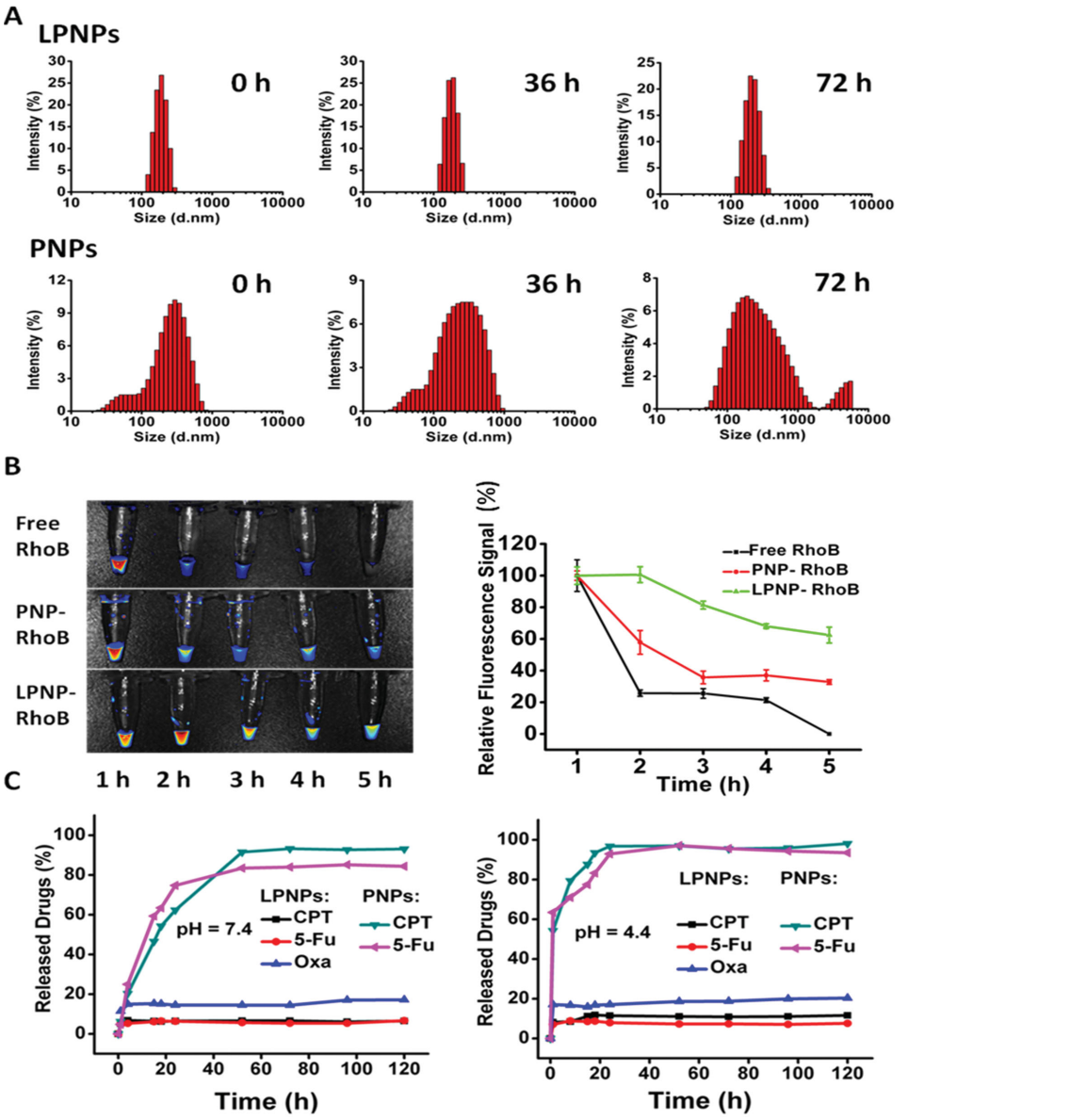

Figure 2. Nanoparticles stability in serum and in vivo and drug release profiles at different pHs. A) The effect of serum on the size distribution of LPNPs and PNPs over time at room temperature. B) Fluorescence images of blood drawn from the mice injected with free RhoB, PNP-RhoB, or LPNP-RhoB (left). The fluorescence intensities of the blood samples were quantified at 1, 2, 3, 4, and 5 h after injection (right). C) Drug release profiles of LPNP-5-Fu-CPT-Oxa and PNP-5-Fu-CPT at pH 7.4 and pH 4.4 at room temperature.

released from PNP-5-Fu-CPT after 2–3 days. In contrast, LPNP-5-Fu-CPT-Oxa lost only a small proportion (less than 20%) of their cargoes over 5 days at both pH 7.4 and 4.4. Thus, these nanoparticles appear to be insensitive to their external environment. The lipid bilayer shell may prevent small drug molecules from freely diffusing out of the polymeric core, and a decreased rate of hydrolysis of the mPEG-PLA polymers may reflect reduced water penetration into the polymeric core, which would be consistent with slower drug release from the nanoparticles.

The high stability of LPNPs at pH 4.4 in solution raises the question of whether the drugs loaded into the LPNPs will be released when they enter cells. To investigate this, we replaced Oxa and 5-Fu in the LPNPs with the green dye fluorescein isothiocyanate (FITC) and the red dye rhodamine B (RhoB) (LPNP-FITC-RhoB). MiaPaCa-2 cells (a human pancreatic ductal carcinoma cell line) were incubated with LPNP-FITC-RhoB and then examined at various time points by confocal microscopy to determine the intracellular distribution of the fluorescent compounds. As shown in **Figure 3**A, the cellular fluorescent intensity increased over time, suggesting that the LPNPs were internalized continuously. At 0.5 h, the major fluorescence signal was orange (indicated by arrows in Figure 3A), consistent with the overlapping fluorescence of the red and green dyes. Compared to free FITC and RhoB group, the fluorescence signal was stronger, indicating that LPNPs enhance uptake of

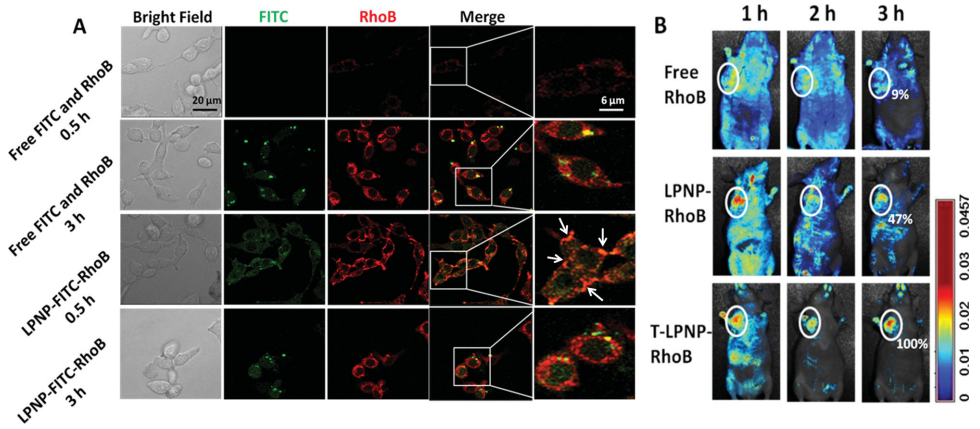

Figure 3. Fluorescent images of LPNP-FITC-RhoB in cells and in vivo imaging and tumor targeting of free RhoB, LPNP-RhoB, and T-LPNP-RhoB. A) In vitro fluorescence images of MiaPaCa-2 cells after incubation with LPNP-FITC-RhoB for 0.5 or 3 h to measure intracellular drug release profiles. As control, the cells were incubated with free FITC and RhoB. B) Whole body dorsal fluorescence images of nu/nu mice bearing subcutaneous tumors at different time points after the administration of free RhoB, LPNP-RhoB, or T-LPNP-RhoB by tail vein injection. Free RhoB was distributed throughout the body. LPNP-RhoB and T-LPNP-RhoB were selectively enriched in the tumor region, with T-LPNP-RhoB showing greater accumulation in the tumor. The tumor sites were marked by white circles. The fluorescent intensities in the tumor site at 3 h were quantitatively analyzed, and the intensity in T-LPNP-RhoB group was normalized as 100%. The result is representative one of the 3 repeated experiments.

dyes. As time progressed (3 h), however, separate red and green fluorescence became increasingly apparent at various locations inside the cells in LPNP-FITC-RhoB group. We also observed the separate fluorescence when three dyes (hydrophilic FITC, Cy5.5, and hydrophobic CPT) were encapsulated into LPNPs (Figure S5, Supporting Information). These data suggest that internalized LPNPs were broken down in cells to release their cargoes. Since the in vitro results (Figure 2C) suggest that LPNPs possess excellent stability in acidic lysosomes (pH 4.4), it is possible that enzymatic hydrolysis of the nanoparticles may be involved in the disassembly and degradation of LPNPs. There are phospholipases in the lysosomes which can degrade outer lipid bilayer.[34] Once the outer lipid shell is degraded, the cathepsin B in lysosomes may permeate into the polymeric core to degrade PEG.[35] Although there is no specific lysosomal enzymes which have been reported responsible for the degradation of PLA, biodegradation of PLA has been studied by esterases, proteases, and lipases secreted from microorganisms.[36,37]

2.4. Targeting Ligands RGD Conjugation and Accumulation of Nanoparticles at the Tumor Sites In Vivo

The ability to decorate the surface of LPNPs with specific targeting ligands represents a major advantage of this technology. In this study, we covalently conjugated tumor targeting RGD polypeptide to the tails of DSPE-PEG through maleimide-thiol coupling to enhance targeting efficiency of the LPNPs.[31] HPLC analysis was used to monitor the efficiency of RGD binding (Figure S6, Supporting Information). The characteristic peak of free RGD was at the beginning of the reaction, but quickly disappeared as the reaction progressed. We next demonstrated the suitability of these decorated nanoparticles for targeted cargo delivery in vitro. The RGD polypeptide specifically binds to *avb*3 integrin which is overexpressed by most cancer cells.[31,38] The overexpression of integrin $\alpha v\beta 3$ in cell membrane of MiaPaCa-2 cells was verified by immunofluorescence imaging (Figure S7, Supporting Information). FITC was encapsulated within the hybrid NPs to enable fluorescent imaging in vitro. We incubated MiaPaCa-2 cells with LPNP-FITC (LPNPs encapsulating FITC) or T-LPNP-FITC (T-LPNPs encapsulating FITC) at 4 °C. At this temperature, the nanoparticles will bind to the cells but will not be internalized. Figure S8, Supporting Information, shows that T-LPNP-FITC accumulated on the plasma membrane of the cells, but LPNP-FITC did not. These results demonstrate that the targeting polypeptide RGD modification endowed T-LPNPs with the ability to target tumor cells in vitro.

To investigate whether the T-LPNPs could target tumors in vivo, we established a subcutaneous tumor-bearing mouse model by inoculating MiaPaCa-2 cells into the upper right abdominal flank of 6–8 week old female BALB/c nu/nu mice. Tumor-bearing mice were sorted into four groups and injected with saline, free RhoB, LPNP-RhoB (RhoB-encapsulated LPNPs), or T-LPNP-RhoB (RhoB-encapsulated T-LPNPs). Fluorescence signals were recorded 1, 2, and 3 h after injection with a Maestro™ in vivo optical imaging system. As shown in Figure 3B, free RhoB initially distributed throughout the body, but then was rapidly degraded and/or cleared. Both LPNP-RhoB and T-LPNP-RhoB tended to accumulate at the site of the tumors, but T-LPNP-RhoB accumulated more strongly at this site and the particles were retained at the tumor site for longer, with much more weak non-specific targeting signal (Figure 3B). At 3h, the fluorescent intensity at tumor region in T-LPNP-RhoB group was more than double of that in LPNP-RhoB group (100% vs 47%). These results indicate that T-LPNPs preferentially accumulate at the site of the tumor relative to LPNPs and free drugs, likely mediated through the active targeting motif.

2.5. Cytotoxicity Effects In Vitro

Having established that T-LPNPs were able to effectively target tumors in vivo, we needed to determine whether T-LPNPs loaded with various chemotherapeutic agents were

efficacious in tumor therapy and whether synergies could be gained by the co-delivery of multiple drugs (5-Fu, CPT, and Oxa) in a single particle. First, we performed CCK-8 viability assays and determined that the most effective molar ratio of 5-Fu: Oxa: CPT for killing MiaPaCa-2 cells was 1: 2: 1 (Figure S9, Supporting Information). Next, MiaPaCa-2 cells were treated with free or T-LPNP-encapsulated drugs (T-LPNP-Drugs) for 12, 24, 36, or 48 h, followed by quantification of cell viability using the CCK-8 assay. The same total drug concentration was used (0.5×10^{-6} M 5-Fu, 1.0×10^{-6} M Oxa, and 0.5×10^{-6} M CPT) for each treatment (**Figure 4**A). T-LPNPs alone exhibited no significant cytotoxicity to MiaPaCa-2 cells, but T-LPNP-Drugs were highly cytotoxic than free drugs at the 24, 36, and 48 h treatment. These results supported our hypothesis that T-LPNPs encapsulation could enhance the cytotoxicity of FOLFIRINOX in vitro. Considering LPNPs can accelerate the cell uptake of the loaded dyes in a short period of time (0.5 h, Figure 3A), we hypothesize that the change of cell internalization pathway of the loaded drugs may play an important role in the enhanced cytotoxicity of T-LPNP-Drugs.[39,40] In addition, unlike the free drugs, the drugs encapsulated in the nanoparticles can be co-delivered into each individual cell simultaneously, which can target multiple essential tumoral metabolic pathways and may enhance the sensitivity of the tumor cells to the chemotherapeutics. However, the underlying mechanism of the increased cytotoxicity of T-LPNP-drugs still need be further explored.

2.6. Antitumor Effect In Vivo

To investigate whether the encapsulation of the FOLFIRINOX drugs into T-LPNPs could enhance their antitumor effects in vivo, we took BALB/c nu/nu mice with MiaPaCa-2 subcutaneous xenografts and divided them into five groups: saline, T-LPNPs, free drugs, LPNP-Drugs, and T-LPNP-Drugs ($n = 5$, 10 μmol kg^{-1}; 5-Fu: Oxa:CPT = 1:2:1). When the tumors reached a predetermined size (33–38 mm^3, approximately 20 days after the tumor cells inoculation), we began the intravenous injection of the drug preparations (or saline) and continued these on every second day thereafter. In the saline and the T-LPNPs group, tumors grew progressively and rapidly (Figure 4B). The unencapsulated antitumor drugs reduced tumor growth to a certain degree, and the LPNP-Drugs group showed an even slower growth. However, the most dramatic inhibition of tumor growth was seen in the T-LPNP-Drugs group. Consistent with the growth curves, the mean weight of the tumors in the T-LPNP-Drugs group was the lowest of all the treatments on day 15 (Figure 4C). These results demonstrate that lipid-polymer hybrid nanoparticles with active targeting RGD polypeptide are able to further enhance the antitumor effects of FOLFIRINOX.

The appearance and extent of apoptosis in the tumors after treatment with various drug formulations were analyzed by the terminal deoxynucleotidyl transferase-mediated dUTP nick end-labeling (TUNEL) assay. The apoptotic cells were indicated by arrows in Figure 4D with a brown staining cell nucleus. The apoptotic rates were evaluated using the percentage of apoptotic tumor cells in the total tumor cells. The T-LPNP-Drugs group showed extensive apoptosis (42%), which was more significant than that of LPNP-Drugs group (34%). However, only weak apoptotic signals (27%) were observed in the tumors of mice treated with free drugs (Figure 4D). In the group treated with blank T-LPNPs, only basal level apoptosis (about 15%) was seen. These results suggest that T-LPNP-Drugs exert their effects on tumor cells by inducing tumor cells apoptosis.

2.7. Side Effect In Vivo

To determine whether T-LPNPs encapsulation could decrease the side effect of FOLFIRINOX regimen, we examined the effects of the drug preparations on healthy BALB/c mice with normal immunity. Four groups were studied: saline control, free drugs, T-LPNPs, and T-LPNP-Drugs ($n = 3$). For investigation of the potential side effect, the dose of combined drugs were 20 μmol kg^{-1} (5-Fu:Oxa:CPT = 1:2:1). Drug injections were carried out on days 1, 3, and 5, and on day 6 the animals were euthanized and various organs, whole blood and serum were collected. Only mice treated with free drugs lost a significant amount of weight (**Figure 5**A). To study potential changes in organ morphology, we analyzed the postmortem histopathology of the heart, liver, and kidney. No obvious morphological changes were observed in heart and kidney tissue (Figure S10, Supporting Information). However, compared with other three groups, there was obvious damage in the liver of mice treated with free drugs: decrease in hepatic cells (Figure 5B, hollow arrows) and inflammatory cells infiltration (Figure 5B, black arrows) observed. To further appraise the potential effects of these drug formulations on the heart, liver, and kidney, we carried out serum biochemical tests. No difference was observed for most biochemical indexes (Figure S11, Supporting Information), except two markers of liver function, ALT (alanine transaminase) and AST (aspartate transaminase), which were significantly elevated in the free drugs group (Figure 5C). Importantly, adverse effects on liver morphology and biochemical parameters were not observed in the T-LPNP-Drugs group (Figure 5B,C). These data suggest that the severe liver damage associated with FOLFIRINOX administration was efficiently alleviated through nanocarriers encapsulation.

Since cytotoxic drugs frequently affect the production of various blood cell types in the bone marrow, we also carried out a routine examination of the blood of the mice treated with different drug formulations. Platelets, white blood cells, monocytes, and lymphocytes all decreased significantly in the mice treated with free drugs (Figure 5D), consistent with the extreme damage to the marrow associated with FOLFIRINOX administration.[8] In contrast, there were minimal changes in the different cell types and other markers in the T-LPNP-Drugs group. These data strongly supported our hypothesis that T-LPNPs are able to reduce the unwanted side effects of FOLFIRINOX.

Finally, we examined four cytokines (TNF-α, TGF-β, IFN-α, and IL-6) by enzyme-linked immunosorbent assay (ELISA) to determine whether the T-LPNPs had any adverse effects on the acute immune response. No significant changes in any of the cytokines were observed in response to T-LPNPs administration (Figure S12, Supporting Information), suggesting high safety profiles of the nanomaterials used as drug carriers.

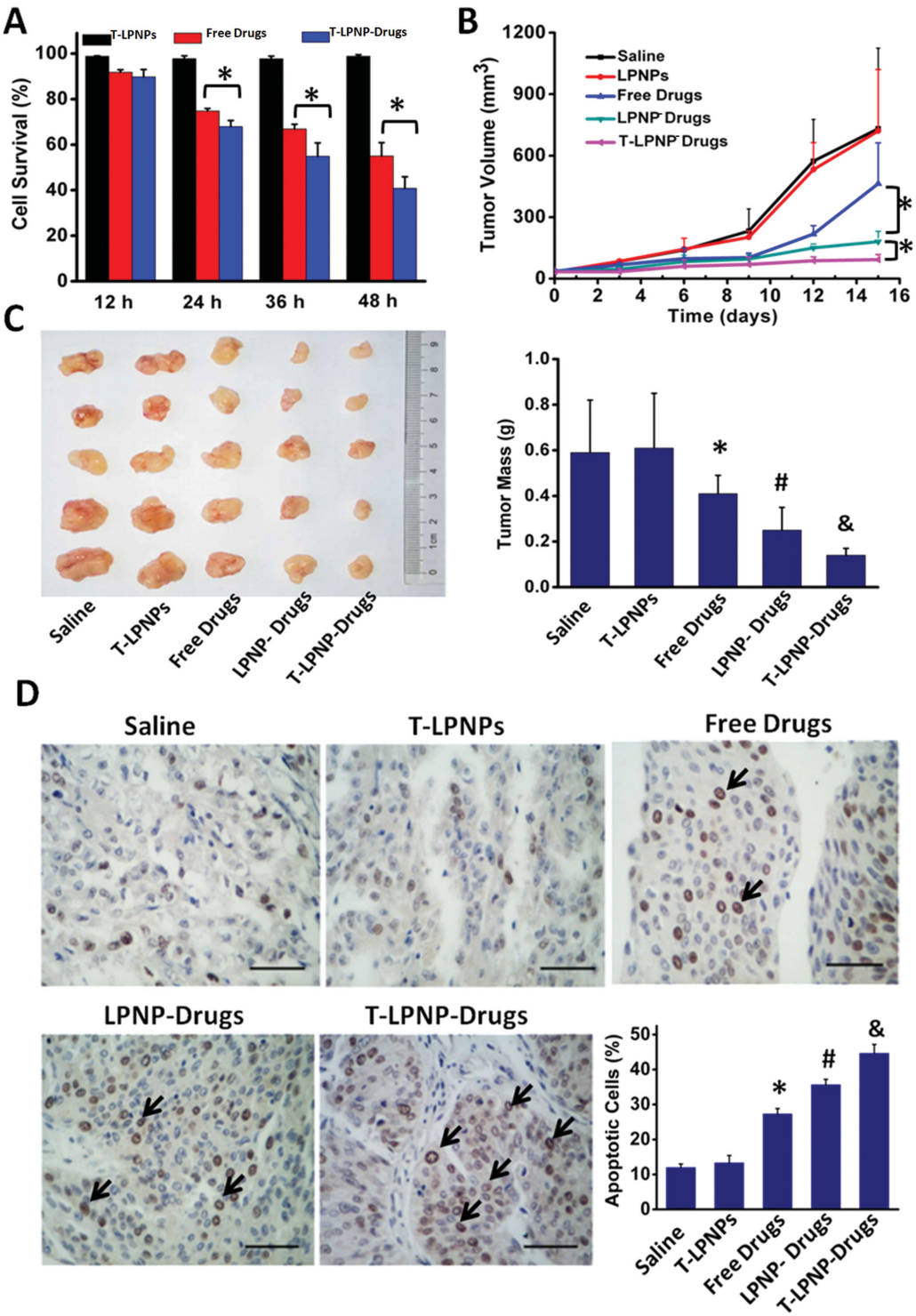

Figure 4. Antitumor activities of T-LPNPs in vitro and in vivo. A) Viability of MiaPaCa-2 cells was assessed using the CCK-8 assay after exposure to T-LPNPs (the drug carriers), free drugs and T-LPNP-Drugs for 12, 24, 36, or 48 h. The total drug concentrations was 2×10^{-6} M, and the 5-Fu:Oxa:CPT weight ratio was 1:2:1. The cell survival ratio was calculated by the following formula: survival ratio (%) = A490 of treated group/A490 of control group × 100%, $^{*}P < 0.05$. B) Tumor growth curves with various drug formulation treatments. Data are presented as mean ± S.D. ($n = 5$), $^{*}P < 0.05$. C) After 15 d, the tumor xenografts were excised, and the tumor weights were measured. $^{*}P < 0.05$ vs saline, $^{\#}P < 0.05$ vs free drugs, $^{\&}P < 0.05$ vs LPNP-Drugs. D) Staining for apoptotic cells (TUNEL assay) in tumor xenografts and quantitative apoptotic cell measurement. The scale bar, 100 μm. Apoptotic cells are indicated by black arrows. The apoptotic rates were evaluated using the percent of apoptotic tumor cells (with a brown staining cell nucleus) in the total tumor cells in each field. Five random fields were observed under a light microscope. Data are presented as mean ± S.D. $^{*}P < 0.05$ vs saline, $^{\#}P < 0.05$ vs free drugs, $^{\&}P < 0.05$ vs LPNP-Drugs.

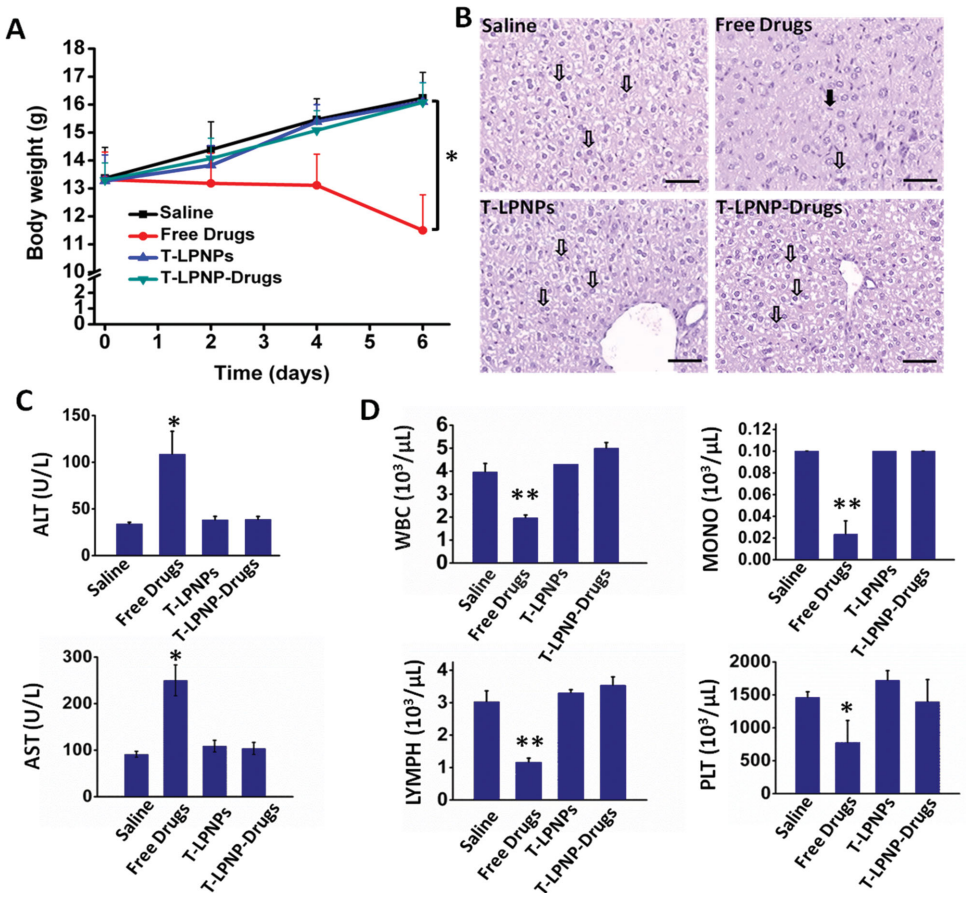

Figure 5. Evaluation of potential side effects of various drug formulations. Healthy BALB/c mice were divided to four groups: saline, free drugs, T-LPNPs, and T-LPNP-Drugs. Drug injections were carried out on days 1, 3, and 5. The mice were euthanized on day 6, and various organs, whole blood and serum were collected. A) Body weight of treated mice as a function of time. $^{*}P < 0.05$. B) Representative H&E staining of liver. Hollow arrows indicated hepatic cells and black arrows indicated inflammatory cells. Scale bar 100 μm. C) Serum biochemical tests ($n = 3$). D) Routine blood examination ($n = 3$). Data are presented as mean ± S.D. $^{*}P < 0.05$. $^{**}P < 0.01$. ALT, alanine transaminase; AST, aspartate transaminase; WBC, white blood cells; MONO, monocytes; LYMPH, lymphocytes; PLT, platelets.

3. Conclusion

In summary, in the current study, we have developed a multiple layer-by-layer lipid-polymer hybrid nanoparticles formulation for simultaneously delivering the three effective constituents of the pancreatic cancer therapeutic FOLFIRINOX regimen. These nanoparticles showed excellent stability both in vitro and in vivo and showed almost no aggregation in serum, leading to prolonged circulation time in vivo. The lipid shell played an important role preventing drug leakage in blood circulation. The incorporation of DSPE-PEG-3400-Mal into the lipid shell and the subsequent linkage of tumor targeting RGD polypeptide to the hybrid nanoparticles enhanced their tumor targeting capability. Due to their longer circulation time and better tumor targeting ability in vivo, T-LPNP-Drugs exhibited significantly improved antitumor efficacy compared with free drugs and further enhancement compared with LPNP-Drugs, with almost no side effects on the major organs in the experimental duration. In contrast, the administration of free FOLFIRINOX led to its well-known toxic effects against the liver and marrow.[8] Compared with the previous nanocarriers,[17,28] the lipid-polymer hybrid nanoparticles displayed great advantages in serum stability, blood circulation time in vivo, controlled drug release, and/or the accumulation ability at tumor sites. The work lays the foundation for the further development of lipid-polymer hybrid nanoparticles for drug delivery for pancreatic cancer therapy.

4. Experimental Section

Assembly of Nanoparticles: mPEG-PLA nanoparticles were prepared by the double emulsion (W/O/W) method with minor modifications.[26] Briefly, 20 mg of mPEG-PLA (molecular weight: 5000–15 000) was dissolved in 1 mL of methylene chloride (containing CPT if required) and 0.2 mL of water (containing 5-Fu if required), and transferred to a centrifuge tube. The mixture was emulsified by sonication for 4 min. The emulsion was added to 2 mL of 2% polyvinyl alcohol (PVA) and emulsified for a second time by sonication for 5 min. The emulsion was then slowly dropped into 10 mL of 0.6% PVA and stirred for 10 min at room temperature. The solvent was be removed by vacuum evaporation. A mixture of phospholipids and cholesterol [lecithin, DSPE-PEG-2000, DSPE-PEG-3400-Mal, and cholesterol in a 60:10:2:15 mass ratio] were dissolved in dichloromethane, and then a lipid film was formed in a round bottom flask under reduced pressure using a vacuum rotary evaporator followed by the addition of the polymer emulsion. Oxa was

added as an aqueous solution if required. The lipid film will coat on the PNPs during sonication for 10 min. DSPE-PEG-3400-Mal was introduced by mixing with lecithin for further functionalization. The targeting cyclic RGD polypeptide was linked to the end of DSPE-PEG-3400-Mal. The resulting hybrid lipid-polymer nanoparticles were collected by centrifugation at 13 000 rpm for 10 min at room temperature and washed twice with distilled water.

Characterizations: TEM measurement, the nanoparticles were negatively stained with 2% uranyl acetate solution, deposited on a carbon-coated copper grid, and examined with a transmission electron microscope (TEM, JEM-200CX, Jeol Ltd., Japan). For dynamic light scattering (DLS) measurement, the size distribution and zeta potential of the nanoparticles was estimated using a Zetasizer Nano ZS90 (Malvern Instruments, Malvern, UK) with 90° optics and a He-Ne Laser (4.0 mW, 633 nm).

HPLC Analysis: Briefly, a Waters HPLC system, composed of an auto sampler (model 717 plus), binary pump (model 1525), UV photodiode array detector (model 996) was used. Samples were applied to a Symmetry C18 reverse phase column (20 μL, 4.6 × 150 mm) and eluted using an acetonitrile, water, trifluoroacetic acid gradient. The starting mobile phase was acetonitrile 5%, water 95%, trifluoroacetic acid (0.1% v/v), with a linear progression linearly to 80% acetonitrile over 25 min. The mobile phase composition was then kept constant at 5% acetonitrile for 1–3 min, followed by a further linear change up to 95% acetonitrile. The flow rate was 1.0 mL/min and the eluent was monitored at 270, 360, and 260 nm for 5-Fu, CPT, and Oxa, respectively. All separations were performed at room temperature.

Encapsulation Efficiency Calculations: The encapsulation efficiency of the LPNPs was calculated by the following equation. Encapsulation Efficiency = $(A–B)/A \times 100\%$, where A is the initial amount of drug added in the system and B represents the amount of drug obtained in the supernatant of the after centrifugation determined by HPLC.

Cell Culture: The human pancreatic ductal adenocarcinoma (PDAC) cell line MiaPaCa-2 was cultured in Dulbecco's modified Eagle's medium (DMEM) (SH30022.01B; Thermo Inc., Bremen, Germany), supplemented with 10% fetal bovine serum at 37 °C in a humidified atmosphere containing 5% CO_2.

In Vitro Cytotoxicity Studies: For the in vitro cell viability assay, MiaPaCa-2 cells were seeded into 96-well plates at a density of 5000 cells per well. Twelve hours after seeding, the cells were treated with various drug formulations for up to a further 48 h. The final total concentration of the three drugs was 2×10^{-6} M. The proportion of viable cells was evaluated using a CCK-8 assay according to the manufacturer's instructions (Dojindo, Japan).

In Vitro Imaging of Tumor Cells: MiaPaCa-2 cells were seeded onto a 35 mm borosilicate chambered cover glasses (Nunc, USA.) at a density of 2×10^5 cells/well and grown at 37 °C for 12 h. The medium was then replaced with 2 mL of fresh medium containing LPNPs loaded with FITC and RhoB. The green dye FITC and the red dye RhoB replaced 5-Fu and Oxa in the LPNPs. After incubation at 37 °C for different times, the cells were washed three times with PBS and were observed with an LSM 710 confocal microscope (Carl Zeiss, USA) at 60× magnification. The excitation wavelengths of FITC and RhoB were 490 and 540 nm respectively, and the emission filters were 525 and 625 nm. In vivo fluorescent images of BALB/c nu/nu mice with tumor xenograft were obtained using a Maestro™ in vivo spectrum imaging system (CRi, Woburn, MA) at an excitation: emission of 540: 625 nm after RhoB-encapsulated T-LPNP injection. The fluorescent intensities in the tumor site at 3h were quantitatively analyzed, and the intensity in T-LPNP-RhoB group was normalized as 100%.

Xenograft Tumor Model in Nude Mice and in Vivo Treatment with Chemotherapeutic Agents: To study the efficacy of the chemotherapeutic drug formulations in vivo, pancreatic cancer tumor xenografts were formed in female BALB/C nu/nu mice by injecting 5×10^6 MiaPaCa-2 cells into the right flank (5 mice/group). When the tumor volume reached 33–38 mm^3, 20 μmol kg^{-1} of drugs (5-Fu:Oxa:CPT at 1:2:1 molar ratio, in various drug formulations) were injected through the tail vein every 2 days. Tumor size was measured using traceable digital vernier calipers every 3 days, and tumor volumes were calculated using the formula $V = 1/2ab^2$, where a is the long axis and b is the short axis. Mice with tumor implants were euthanized after 15 d, and the tumor xenografts were excised and weighed. Serum was collected for biochemical tests. The tumor xenografts were sectioned and stained by terminal deoxynucleotidyl transferased dUTP nick end labeling (TUNEL) to determine the level of apoptosis. The apoptotic rates were evaluated using the percent of apoptotic cancer cells (with a brown staining cell nucleus) in the total cancer cells. Five random fields were observed under a light microscope.

Analysis of the Side Effects of Chemotherapeutic Drugs in BALB/c Mice: To study the side effects of various drug formulations, we divided healthy female BALB/c mice into four groups: saline, free drugs, T-LPNPs, and T-LPNP-Drugs ($n = 9$). Drug injections were carried out on day 1, 3, and 5, and body weights of the mice were measured every day. Six mice were euthanized on day 6. In each group, serum was collected from three mice and whole blood from another three, for biochemical tests and routine blood examination respectively. The hearts, livers, and kidneys of treated mice were fixed, sectioned and H & E stained to study potential changes in organ morphology. In addition, the serum from the remaining three mice in the saline and T-LPNPs groups was collected for evaluation of acute immune response. Four acute immune response-related cytokines (TNF-α, TGF-β, IFN-α, and IL-6) were measured by enzyme-linked immunosorbent assay (ELISA, Solarbio S&T Co., Beijing, China).

Statistical Analysis: Statistical analyses were performed using SPSS version 18.0 software (SPSS Inc., Chicago, IL). Student's t-test for unpaired data was used to evaluate statistical differences between mean values. All data are presented as the mean ± standard deviation (SD), and data were considered statistically significant at $P < 0.05$.

Supporting Information

Supporting Information is available from the Wiley Online Library or from the author.

Acknowledgements

This work was supported by MoST 973 (2012CB934004); National Distinguished Young Scientists program (31325010); National Natural Science Foundation of China (81302082, 81272685, 31301151, 31470957, 31471340, 81472264, 81401957, and 81172355); Key Program of Natural Science Foundation of Tianjin (11JCZDJC18400, 13YCYBYC37400); Major Anticancer Technologies R&D Program of Tianjin (12ZCDZSY16700). F.L., X.Z., and H.W. contributed equally to this work.

Received: May 15, 2014
Revised: November 21, 2014
Published online: December 15, 2014

[1] R. Siegel, J. Ma, Z. Zou, A. Jemal, *CA. Cancer J. Clin.* **2014**, *64*, 9.
[2] H. A. Burris, M. J. Moore, J. Andersen, *J. Clin. Oncol.* **1997**, *15*, 2403.
[3] M. Di Marco, R. Di Cicilia, M. Macchini, E. Nobili, S. Vecchiarelli, G. Brandi, G. Biasco, *Oncol. Rep.* **2010**, *23*, 1183.
[4] V. Heinemann, S. Boeck, A. Hinke, R. Labianca, C. Louvet, *BMC Cancer.* **2008**, *8*, 82.
[5] P. A. Philip, J. Benedetti, C. L. Corless, R. Wong, E. M. O'Reilly, P. J. Flynn, *J. Clin. Oncol.* **2010**, *28*, 3605.
[6] M. J. Moore, D. Goldstein, J. Hamm, A. Figer, J. R. Hecht, S. Gallinger, *J. Clin. Oncol.* **2007**, *25*, 1960.
[7] T. Conroy, F. Desseigne, M. Ychou, O. Bouche, *N. Engl. J. Med.* **2011**, *364*, 1817.

[8] S. Gourgou-Bourgade, C. Bascoul-Mollevi, F. Desseigne, M. Ychou, O. Bouche, R. Guimbaud, *J. Clin. Oncol.* **2013**, *31*, 23.
[9] R. Kim, *Lancet Oncol.* **2011**, *12*, 8.
[10] L. V. dos Santos, D. P. de Andrade, J. P. Lima, *J. Clin. Oncol.* **2012**, *30*, 114.
[11] K. K. Jain, *BMC Med.* **2010**, *8*, 83.
[12] F. M. Kievit, M. Zhang, *Adv. Mater.* **2011**, *23*, H217.
[13] K. Rakesh, *Nat. Rev. Clin. Oncol.* **2010**, *7*, 653.
[14] D. D. Von Hoff, T. Ervin, F. P. Arena, E. G. Chiorean, J. Infante, M. Moore, T. Seay, S. A. Tjulandin, W. W. Ma, M. N. Saleh, M. Harris, M. Reni, S. Dowden, D. Laheru, N. Bahary, R. K. Ramanathan, J. Tabernero, M. Hidalgo, D. Goldstein, E. Van Cutsem, X. Wei, J. Iglesias, M. F. Renschler , *N. Engl. J. Med.* **2013**, *369*, 1691.
[15] C. E. Ashley, *Nat. Mater.* **2011**, *10*, 389.
[16] K. Raemdonck, K. Braeckmans, J. Demeester, S. C. De Smedt, *Chem. Soc. Rev.* **2014**, *43*, 444.
[17] S. Mitragotri, J. Lahann, *Adv. Mater.* **2012**, *24*, 3717.
[18] W. W. Wang, D. Cheng, F. M. Gong, X. M. Miao, X. T. Shuai, *Adv. Mater.* **2012**, *24*, 115.
[19] J. A. Barreto, W. O'Malley, M. J. Kubeil, B. Graham, H. Stephan, L. Spiccia, *Adv. Mater.* **2011**, *23*, H18.
[20] T. Ruysschaert, A. F. P. Sonnen, T. Haefele, W. Meier, M. Winterhalter, D. Fournier, *J. Am. Chem. Soc.* **2005**, *127*, 6242.
[21] B. Naeye, H. Deschout, M. Roding, M. Rudemo, J. Delanghe, K. Devreese, J. Demeester, K. Braeckmans, S. C. De Smedt, K. Raemdonck, *Biomaterials* **2011**, *32*, 9120.
[22] B. Naeye, H. Deschout, V. Caveliers, B. Descamps, K. Braeckmans, C. Vanhove, J. Demeester, T. Lahoutte, *Biomaterials* **2013**, *34*, 2350.
[23] M. M. van Schooneveld, E. Vucic, R. Koole, Y. Zhou, J. Stocks, D. P. Cormode, C. Y. Tang, R. E. Gordon, K. Nicolay , A. Meijerink, Z. A. Fayad, W. J. M. Mulder, *Nano Lett.* **2008**, *8*, 2517.
[24] V. P. Torchilin, *Nat. Rev.* **2005**, *4*, 145.
[25] B. Mandal, H. Bhattacharjee, N. Mittal, H. Sah, P. Balabathula, L. A. Thoma, G. C. Wood, *Nanomedicine* **2013**, *9*, 474.
[26] H. Wang, Y. Wu, R. F. Zhao, G. J. Nie, *Adv. Mater.* **2013**, *25*, 1616.
[27] H. Wang, Y. Zhao, Y. Wu, Yu. Hu. G. J. Nie, K. Nan, *Biomaterials* **2011**, *32*, 8281.
[28] I. Ogihara-Umeda, H. Nishigori, in *Microspheres Microcapsules and Liposomes*, (Ed: R. Arshady) Citus Books, London, **2001**, p. 124.
[29] N. Kamaly, Z. Y. Xiao, P. M. Valencia, A. F. Radovic-Moreno, O. C. Farokhzad, *Chem. Soc. Rev.* **2012**, *41*, 2971.
[30] D. Bazile, C. Prud'homme, M. T. Bassoullet, M. Marlard, G. Spenlehauer, M. Veillard, *J. Pharm. Sci.* **1995**, *84*, 493.
[31] C. B. Hansen, G. Y. Kao, E. H. Moase, S. Zalipsky, T. M. Allen, *BBA-Biomembranes* **1995**, *1239*, 133.
[32] T. Yang, C. Lin, J. Zhai, S. Shi, M. Zhu, N. Zhu, J. H. Lu, G. S. Yang, M. C. Wu, *J. Cancer Res. Clin. Oncol.* **2012**, *10*, 1121.
[33] M. Ducreux, E. Mitry, M. Ould-Kaci, V. Boige, J. F. Seitz, R. Bugat, J. L. Breau, O. Bouche, P. L. Etienne, J. M. Tigaud, F. Morvan, E. Cvitkovic, P. Rougier, *Ann. Oncol.* **2004**, *15*, 1577.
[34] T. Kolter, K. Sandhoff, *FEBS Lett.* **2010**, *584*, 1700.
[35] M. Pechar, K. Ulbrich, V. Subr, L. W. Seymour, E. H. Schacht, *Bioconjug. Chem.* **2000**, *11*, 131.
[36] M. S. Shive, J. M. Anderson, *Adv. Drug Deliv. Rev.* **1997**, *28*, 5.
[37] K. Madhavan Nampoothiri, N. R. Nair, R. P. John, *Bioresour. Technol.* **2010**, *101*, 8493.
[38] U. Hersel, C. Dahmen, H. Kessler, *Biomaterials* **2003**, *24*, 4385.
[39] D. Cosco, A. Bulotta, M. Ventura, C. Celia, T. Calimeri, G. Perri, D. Paolino, N. Costa, P. Neri, P. Tagliaferri, P. Tassone, M. Fresta, *Cancer Chemother. Pharmacol.* **2009**, *64*, 1009.
[40] S. Rejiba, L. H. Reddy, C. Bigand, C. Parmentier, P. Couvreur, A. Hajri, *Nanomed-Nanotechnol.* **2011**, *6*, 841.